

Probing EFT breakdown in the tails of W^+W^- observables

Daniel Gillies¹, Andrea Banfi¹, and Adam Martin²

¹Department of Physics and Astronomy, University of Sussex, Brighton BN1 9QH, U.K.

²Department of Physics, University of Notre Dame, Notre Dame, IN 46556, USA

Abstract

In this letter, we test clipping effective field theory (EFT) simulations as a method of ensuring EFT validity. The procedure imposes that, at the level of the simulation, the invariant mass of a W^+W^- pair M_{WW} is less than the new physics scale Λ . We compare this to two other methods, comparison bin by bin of dimension-6 and dimension-8 squared contributions and implementing a cut on data. We find that setting $M_{WW} < \Lambda$ is not strict enough to ensure that the hierarchy of EFT operators is respected for dimension-6 and dimension-8 contributions. We also show that, even when using a stricter cut on M_{WW} , due to different correlations between M_{WW} and $M_{e\mu}$ at different EFT orders, the bins in $M_{e\mu}$ (the invariant mass of the leptons originating from W decays) used in an EFT fit may not truly be in the regime of EFT validity when performing a dimension-6 fit with $M_{WW} < \Lambda$. We also explore the correlations of three transverse mass observables: M_{T1} , M_{T2} and M_{T3} , finding that M_{T1} and M_{T3} follow the M_{WW} distribution more closely than $M_{e\mu}$. We present sensitivity studies using both the M_{T3} distribution and $M_{e\mu}$ distribution. We test implementing an experimental cut on M_{T3} in place of clipping the EFT simulation at $M_{WW} < \Lambda$. We finally comment that adding $M_{WW} < \Lambda$ cuts only to the EFT simulation could be interpreted as modifying the SMEFT expansion by a form factor and could therefore impact the model independence of EFT fits under this procedure.

1 Introduction

Model independent effective field theory (EFT) fits are becoming a more popular method of interpreting collider data [1]. The power of these methods is that the vast space of possible UV complete models is reduced to a finite-dimensional space of possible directions for new physics at first order. These corrections are encoded by operators which have mass dimension $d > 4$. Each operator comes with a Wilson coefficient (c_i), expected to be $O(1)$, which encodes the importance of that operator in the new theory. Each operator is suppressed by a factor of Λ^{d-4} , where Λ is the mass or energy scale of new physics. The EFT expansion is formally in powers of E/Λ , where E is the energy scale of the interaction being considered. If we assume that new physics appears at scales much larger than the energies which can be achieved at current colliders ($E \ll \Lambda$) then this EFT expansion will be valid and therefore useful predictions can be extracted. When $E > \Lambda$ the theory breaks down and is no longer a useful description. The Standard Model Effective Field Theory (SMEFT) is one such theory which will be used to constrain collider data in the near future – at dimension-6 it contains 61 operators (assuming minimal flavour violation) [2]. Performing these fits with total cross-section data is common, and these measurements can be thought to exist at some energy scale related to the process

being considered (e.g. M_Z , M_H , Λ_{EW}). However, in order to better constrain theories, differential cross-section data is also used. When considering high-energy tails of these distributions, it is important to place cuts on the energy of the interaction, E , such that the events being used are those which have energy below the EFT scale being considered. For some observables, the overall energy of an interaction is not directly resolvable due to missing neutrino energy. Methods for ensuring EFT validity in differential distributions are being developed but so far there is no consensus on a universal best method [3].

The production of a pair of EW bosons at the LHC is a very useful process to probe physics beyond the Standard Model (BSM). In particular, the contribution of higher-dimensional non-renormalisable operators tends to grow with energy, so that their effect is expected to become visible in the tail of suitable kinematic distributions. Furthermore, these processes give tree-level access to triple electroweak (EW)-field strength operators (i.e. those $\propto WWW$) [4–7]. Importantly, when viewed inclusively, SMEFT WWW does not interfere well with the Standard Model (SM) so the first place this operator appears is at dimension-6 squared [5, 8]. This makes studies aimed at WWW particularly susceptible to contamination from dimension-8 and other higher order effects [9, 10]. One such diboson process is W^+W^- (WW) production which as been measured at the LHC in several analyses [11–19].

This process is technically more challenging to describe than others, due to the need to restrict the phase space available to accompanying jets in order to suppress the otherwise overwhelming top-antitop background. The quantity that is mostly sensitive to high energy BSM physics would be the distribution in the diboson invariant mass M_{WW} . However, this quantity is not accessible at colliders (due to the missing neutrino energy), so appropriate proxies need to be identified. Typically, one sets constraints on higher-dimensional operators by looking at (possibly alongside other angular distributions) the distribution in $M_{e\mu}$, the invariant mass of the electron and the muon arising from the decay of the two W bosons. This has been done in several EFT analyses of the channel [11, 12, 20–23]. However, it has already been shown previously that $M_{e\mu}$ does not correlate well with M_{WW} and so should not be used directly to set EFT validity (e.g. implementing a cut $M_{e\mu} < \Lambda/2$ on data) [23].

In previous work, we noted that, since WW production via gluon fusion is very suppressed in the SM, the interference between dimension-8 $GGWW$ EFT operators and the SM can be considered negligible in the large $M_{e\mu}$ limit [24]. We used this fact to argue that EFT fits including the square of dimension-6 operators can be safely performed (for the gg channel) without including the interference of the SM with dimension-8 operators, which are formally of the same order ($1/\Lambda^4$).

This argument holds provided the EFT expansion itself is valid. The EFT regime is formally established by having $M_{WW} \ll \Lambda$. However, as mentioned earlier, this quantity is not available at colliders. We directly compared, bin by bin, the squared contributions from the leading bosonic dimension-6 and dimension-8 operators to determine, for a given value of Λ , the range of $M_{e\mu}$ bins over which the EFT expansion remains convergent. The procedure involved including only the bins where the largest dimension-6 squared contribution ($\sigma^{(6)}$) was at least twice as large as the largest dimension-8 contribution ($\sigma^{(8)}$) or:

$$\frac{(2 \text{ TeV})^8 \sigma_{\Lambda=2 \text{ TeV}}^{(8)}}{\Lambda^8} = \frac{1}{2} \frac{(2 \text{ TeV})^4 \sigma_{\Lambda=2 \text{ TeV}}^{(6)}}{\Lambda^4}, \quad (1.1)$$

in the assumption that all the coefficients of the higher-dimensional operators were of order one [24]. To obtain numerical estimates, we computed cross-sections at a reference value of $\Lambda = 2 \text{ TeV}$. This led to the condition that a bin should only be used when the EFT scale Λ being probed is greater than Λ_{\min} , where

$$\Lambda_{\min} = (2 \text{ TeV}) \left(2 \times \frac{\sigma_{\Lambda=2 \text{ TeV}}^{(8)}}{\sigma_{\Lambda=2 \text{ TeV}}^{(6)}} \right)^{\frac{1}{4}}. \quad (1.2)$$

An alternative strategy employed elsewhere does not consider the $M_{e\mu}$ bins at all. Rather, the dimension-6 interference and squared contributions are computed with a leading-order (LO) event generator with the constraint that $M_{WW} < \Lambda$ [3, 11, 23]. Adding this constraint is formally equivalent to modifying the SMEFT Feynman rules for a dimension-6 operator with Wilson coefficient c_i as follows:

$$\frac{c_i}{\Lambda^2} \rightarrow \frac{c'_i}{\Lambda^2} \Theta(1 - p^2/\Lambda^2), \quad (1.3)$$

The step function is applied only to the simulation of the dimension-6 contribution, not the SM contribution or the data, which means that we are no longer strictly fitting SMEFT dimension-6 operators. In fact, if we replace the step function in eq. (1.3) with a smooth form factor $\mathcal{F}(p^2/\Lambda^2)$ that suppresses higher values of p^2 , this would correspond to an infinite series of higher dimensional operators, which means we are no longer truncating the EFT expansion at dimension-6. The step function in eq. (1.3) is not smooth and does not permit an expansion in p^2/Λ^2 . However, it is hoped that fitting c'_i to the data should give some indication of what value c_i could be constrained to in the EFT valid regime. A cleaner method might be to still fit c_i to the data with the standard dimension-6 SMEFT operator but to only use regions of phase space (or bins) where including the step function has a small impact. In this paper, we do not consider this latter method further and we just compare to what is currently used in recent experimental analyses, which is to fit on c'_i [11].

There, it is assumed that, with the cut on M_{WW} at the generator level, the dimension-6 operators will only produce meaningful contributions in those $M_{e\mu}$ bins for which M_{WW} is within the EFT validity regime. However, with either of the two above methods, there is no guarantee that the selected $M_{e\mu}$ bins will not receive contributions from higher dimensional (8 or higher) operators at larger values of M_{WW} . This is because these higher-dimensional operators can grow faster with energy than dimension-6 operators, so events with larger values of M_{WW} can have larger cross-sections, and hence have a bigger impact at lower values of $M_{e\mu}$.

More precisely, we wish to understand what the expected value of M_{WW} is for a given $M_{e\mu}$ – i.e $\mathbb{E}[M_{WW} | M_{e\mu}]$. This quantity gives us an indication of the minimum EFT scale Λ that is required for each bin $M_{e\mu}$. If this quantity changes as we include higher orders in the EFT, then the $M_{e\mu}$ bins which are included in the dimension-6 squared prediction could have large higher-order EFT contributions which are not accounted for.

In this letter, we want to compare the method of fitting $\frac{c'_i}{\Lambda^2} \Theta(1 - p^2/\Lambda^2)$ to alternatives and interpret the outcome by explicitly studying the correlation between $M_{e\mu}$ and M_{WW} . For this study, we choose the bosonic dimension-6 and dimension-8 operators that give the largest contributions to the gg -channel. They are

$$\begin{aligned} \mathcal{O}_{GH}^{(6)} &\equiv H^\dagger H G_{\mu\nu}^a G^{a,\mu\nu}, \\ \mathcal{O}_3^{(8)} &\equiv G_{\mu\nu}^a \tilde{G}^{a,\mu\nu} W^{I,\rho\sigma} \tilde{W}_{\rho\sigma}^I. \end{aligned} \quad (1.4)$$

where $G_{\mu\nu}^a$ and $W_{\rho\sigma}^I$ are the gluon and W field-strength tensors, and $\tilde{T}_{\mu\nu} = \frac{1}{2}\epsilon_{\mu\nu\rho\sigma}T^{\rho\sigma}$ the dual of any tensor $T^{\mu\nu}$. Finally, we will also study the correlation of M_{WW} to other transverse-mass observables which should more closely follow M_{WW} , to see if observables which are more correlated to M_{WW} give better constraints than those obtained with $M_{e\mu}$.

WW production in the SM is dominated by $q\bar{q}$ -initiated amplitudes, whilst this study focuses exclusively on bosonic operators which enter into the gg -channel. The philosophy advocated for in this paper is that, for the EFT to be valid, one should check its validity for all processes, not just those which dominate the cross-section. Not doing so assumes that the expansion for $q\bar{q}$ operators is different to that of the gg operators (i.e. that gg operators are suppressed relative

to $q\bar{q}$ operators as $\Lambda_{gg} \gg \Lambda_{q\bar{q}}$ or $(c_i)_{q\bar{q}} \gg (c_i)_{gg}$). Note that we ourselves do not consider here the fermionic and $q\bar{q}$ -operators as well as some higher order SM effects, therefore the constraints from this paper should be treated as purely illustrative.

2 Comparison of EFT Validity Methods

In this section, we want to compare methods of ensuring fits of Wilson coefficients are performed only on bins which are within the EFT validity regime for a given Λ . At the very least, this should require that dimension-8 squared contributions are negligible compared to the dimension-6 squared contributions for the kinematical values of the data points.

We consider a simplified model with just the most significant dimension-6 and dimension-8 operators as in eq. (1.4) as BSM contributions:

$$\mathcal{L} \supset \mathcal{L}_{\text{BSM}} = \frac{c_{GH}^{(6)}}{\Lambda^2} G_{\mu\nu}^a G^{a,\mu\nu} + \frac{\tilde{c}_{GH}^{(6)}}{\Lambda^2} G_{\mu\nu}^a \tilde{G}^{a,\mu\nu} + \sum_i \frac{c_3^{(8)}}{\Lambda^4} G_{\mu\nu}^a \tilde{G}^{a,\mu\nu} W^{I,\rho\sigma} \tilde{W}_{\rho\sigma}^I. \quad (2.1)$$

We can then determine a BSM contribution to the amplitude needed to compute physical distributions as:

$$\mathcal{M}_{\text{BSM}} = \frac{c_{GH}^{(6)}}{\Lambda^2} \mathcal{M}_g^{(6,gg)} + \frac{\tilde{c}_{GH}^{(6)}}{\Lambda^2} \tilde{\mathcal{M}}_g^{(6,gg)} + \frac{c_3^{(8)}}{\Lambda^4} \mathcal{M}_3^{(8,gg)}. \quad (2.2)$$

These terms may either be squared or interfered with SM gg production. Both of these contributions at dimension-6 and dimension-8 are available at LO and next-to-leading logarithmic (NLL) accuracy (when resummed with a jet-veto $p_{T,\text{veto}}$) in MCFM-RE [24–28]. For the numerical results in this letter, we consider WW production at the HL-LHC, with fiducial cuts based on the ATLAS study in [14]. These are summarised in table 1. Unless specified otherwise, we use the “NNPDF31_nnlo_as_0118_luxqed_nf_4” PDF set [29]. Where mentioned, we use the “NNPDF40_nnlo_as_01180_nf_4” PDF set due to better accuracy in the high- x region [30].

Fiducial selection requirement	Cut value
p_T^ℓ	$> 27 \text{ GeV}$
$ y_\ell $	< 2.5
$M_{e\mu}$	$> 55 \text{ GeV}$
$ \vec{p}_T^e + \vec{p}_T^\mu $	$> 30 \text{ GeV}$
Number of jets with $p_T > 35 \text{ GeV}$	0
\cancel{E}_T	$> 20 \text{ GeV}$

Table 1: Definition of the $WW \rightarrow e\mu$ fiducial phase space, where \vec{p}_T^ℓ, y_ℓ are the transverse momentum and rapidity of either an electron or a muon, $M_{e\mu}$ is the invariant mass of the electron-muon pair, and \cancel{E}_T is the missing transverse energy.

As anticipated in the introduction, the interference between dimension-8 contributions and the SM is negligible. Therefore, we concentrate here on the squared contributions of individual operators. These are obtained from MCFM-RE and shown in figure 1.

We consider three classes of methods of ensuring this EFT validity as follows:

- **Clipping on Simulation (CoS).** By “Clipping” on the simulation, we refer to the method of enforcing $M_{WW} < \Lambda$ on the EFT simulation alone, which is equivalent to fitting Wilson coefficients as $\frac{c_i}{\Lambda^2} \Theta(1 - p^2/\Lambda^2)$. This is achieved by setting a cut in the generation of the BSM prediction. However, since the cut is not actually placed on the data, the SM simulation is run as normal without the cut on M_{WW} .

- **Comparison bin-by-bin of dimension-6 and dimension-8 operators (CBB).** This method involves directly comparing the size of dimension-6 and dimension-8 operators. Using the relation in eq. (1.2), this is used to find the range of bins in a distribution where the dimension-8 squared contribution is negligible compared to the dimension-6 squared contribution. Assuming accurate modelling of both contributions, this method automatically satisfies our definition of ensuring that data used falls within the EFT valid regime.
- **Implementing a cut on data (CoD).** The alternative method would be to implement a cut on the data itself which removes events with energies above the cut-off scale Λ . Since M_{WW} is not observable in this channel, a suitable proxy must be identified. $M_{e\mu}$ has already been shown to be a poor proxy for M_{WW} [23] but one could use other observables such as transverse-mass variables.

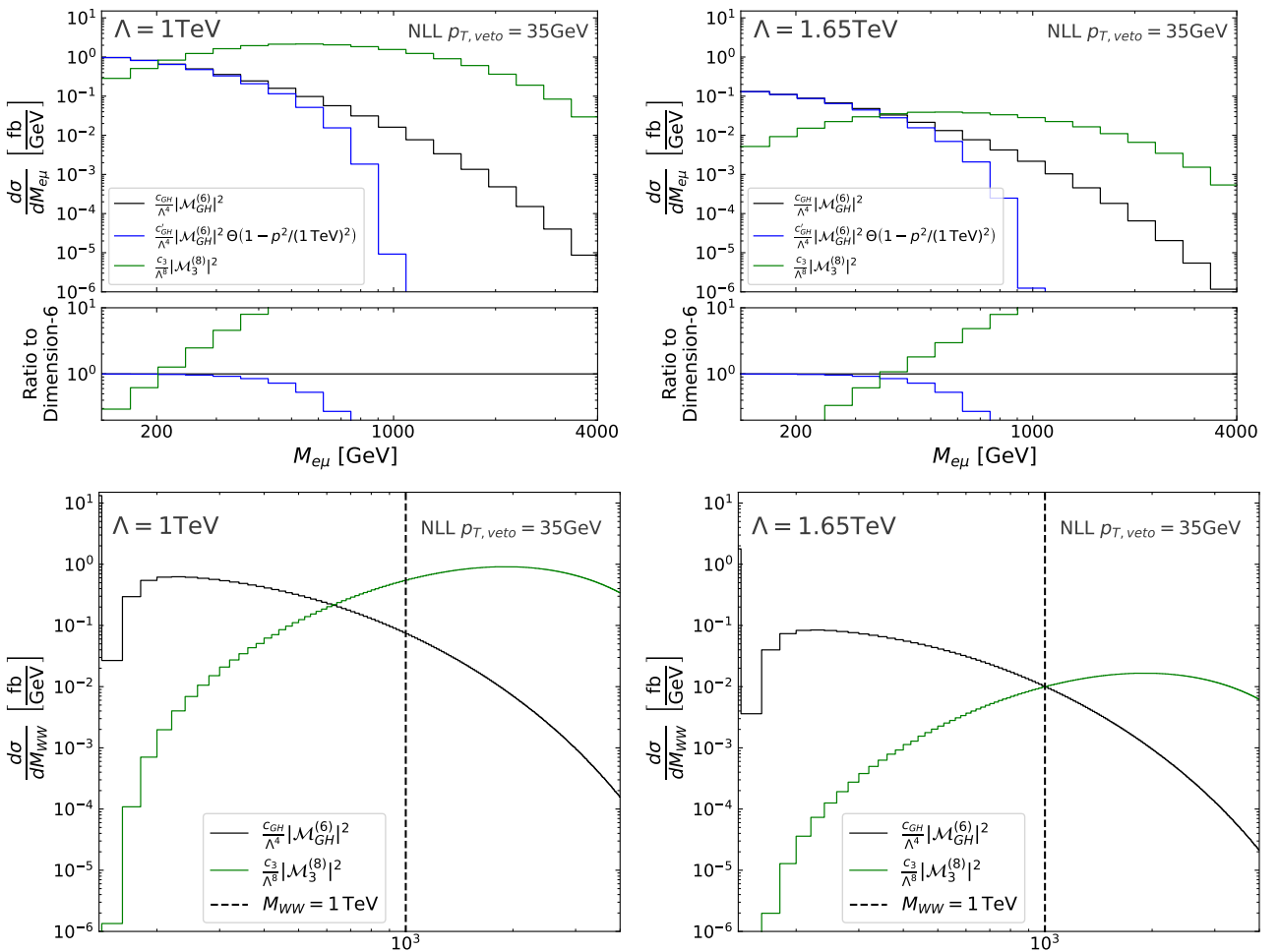


Figure 1: Comparison of the full dimension-6 (black), dimension-6 subject to the cut $M_{WW} < 1$ TeV (blue), and dimension-8 (green) contributions to the $M_{e\mu}$ (left) and M_{WW} (right) distributions. The upper panels are for $\Lambda = 1$ TeV, the lower panels for $\Lambda = 1.65$ TeV.

In figure 1, we test the CoS method via comparison with the CBB method, which we assume to be the most robust way of ensuring EFT validity and has already been used in [24]. When comparing to dimension-8 squared contributions we always perform simulations without a cut. This is because the cut does not appear in the data and is only a method to reduce the size of dimension-6 contributions in bins where dimension-8 dominates. From the upper left-hand panel of figure 1, it can be seen that imposing CoS with $M_{WW} < 1$ TeV for $\Lambda = 1$ TeV does

not remove $M_{e\mu}$ bins where dimension-8 squared dominates ($M_{e\mu} > 200$ GeV). Specifically, the range $200 \text{ GeV} < M_{e\mu} < 400 \text{ GeV}$ still has a significant dimension-8 squared contribution even after CoS. This implies CoS is not a good method for determining the range of EFT validity. There are two main reasons for this. One is the fact the cut $M_{WW} < \Lambda$ is not strict enough. As can be seen from the lower panels of figure 1, for a cut of $M_{WW} < 1 \text{ TeV}$ to be effective, Λ must be at least 1.65 TeV . The second reason is that, even when applying this stricter cut, the correlation between $M_{e\mu}$ and M_{WW} can change order by order in the EFT expansion. In fact, as we add higher-order terms in the EFT expansion, amplitudes grow more and more rapidly with energy. We expect high M_{WW} bins to overcome kinematical barriers and contribute more and more to lower energy $M_{e\mu}$ bins. Therefore, using dimension-6 predictions to estimate the contribution of higher dimensional operators is not an effective strategy. This can be seen in the upper right-hand panel of figure 1, where CoS with $M_{WW} < 1.65 \text{ TeV}$ for $\Lambda = 1 \text{ TeV}$ does not eliminate bins in the $M_{e\mu}$ distribution where dimension-8 squared dominates.

Although CBB is definitely more robust than CoS, it can be more cumbersome to implement in practice. Firstly, it requires knowledge of the largest dimension-8 contributions. Second it requires re-evaluating which bins can be used for every value of Λ . Therefore, it would be desirable to have a good measurable proxy for M_{WW} which implement a robust CoD procedure. This will be discussed in the following section.

3 Transverse-Mass Observables

To confirm the changing relationship between $M_{e\mu}$ and M_{WW} (and that therefore $M_{e\mu}$ is not a good proxy for M_{WW}), we compute $\mathbb{E}[M_{WW} | M_{e\mu}]$, the conditional expectation value of M_{WW} for a given $M_{e\mu}$ bin. We repeat this for the SM, dimension-6, and dimension-8 squared contributions. Since the distribution of M_{WW} for a given $M_{e\mu}$ bin is skewed, we use the asymmetric variance to obtain an error on $\mathbb{E}[M_{WW} | M_{e\mu}]$.

The conditional expectation value $\mathbb{E}[M_{WW} | M_{e\mu}]$ (along with an error from its asymmetric variance) is shown in the upper-left panel of figure 2 at NLL accuracy for the SM gg contribution, the dimension-6 ($\phi^\dagger \phi GG$) and dimension-8 ($WWGG$) squared contributions. The expected M_{WW} is plotted for 18 logarithmically spaced bins from $138 < M_{e\mu} < 4000$ GeV. For all the expectation value plots in this section, we use the “NNPDF40_nnlo_as_01180_nf_4” PDF set [30].

In the SM, there is a strong correlation between $M_{e\mu}$ and M_{WW} with $M_{e\mu} \approx \frac{3M_{WW}}{4}$. In fact, the SM cross-section falls rapidly with energy, both due to phase-space constraints and the effect of the jet veto. Whilst we might naïvely expect on average $M_{e\mu} \approx \frac{M_{WW}}{2}$, the rapidly decaying nature of the cross-section means that lower energy M_{WW} bins will contribute more, which skews the average closer to $M_{e\mu} = M_{WW}$. At dimension-6, there is still some correlation between $M_{e\mu}$ and M_{WW} . However, the relation between the two changes as the dimension-6 contribution no longer decreases as rapidly with energy compared to the SM. As a consequence, we now get much closer to the naïve expectation $M_{e\mu} \approx \frac{M_{WW}}{2}$. At dimension-8, there is a much greater variance, showing that the correlation between M_{WW} and $M_{e\mu}$ is weaker. Furthermore, given an $M_{e\mu}$ bin, the events which contribute have a much higher M_{WW} value for dimension-8. In this case, the relation at lower $M_{e\mu}$ is $M_{e\mu} \approx \frac{M_{WW}}{4}$ for lower $M_{e\mu}$ values. Note that, for all distributions, $\mathbb{E}[M_{WW} | M_{e\mu}]$ converges to $M_{e\mu} = M_{WW}$ at the 14 TeV kinematical barrier.

To summarise, the dimension-8 correlation differs quite substantially from that of the dimension-6 contribution. Lower $M_{e\mu}$ bins do not get as much contribution from high- M_{WW} events in the dimension-6 case when compared to the dimension-8 case. The fact that $M_{e\mu}$ and M_{WW} correlate poorly means that the EFT breakdown happens at very low energies for the $M_{e\mu}$ observable. With this in mind, we try to find better observables which could more closely track M_{WW} , which we remind is not observable for leptonic W decays.

In the literature [25], we found three transverse-mass observables which were designed to act as a good proxy of the M_{WW} distribution. These are defined as:

$$M_{T1} \equiv \sqrt{(M_{T,e\mu} + \not{p}_T)^2 - (\vec{p}_{T,e\mu} + \vec{\not{p}}_T)^2}, \quad (3.1a)$$

$$M_{T2} \equiv \sqrt{2p_{T,e\mu} \not{p}_T (1 - \cos \Delta\phi_{e\mu,\text{miss}})}, \quad (3.1b)$$

$$M_{T3} \equiv \sqrt{(M_{T,e\mu} + \not{M}_T)^2 - (\vec{p}_{T,e\mu} + \vec{\not{M}}_T)^2}, \quad (3.1c)$$

with

$$M_{T,e\mu} \equiv \sqrt{p_{T,e\mu}^2 + M_{e\mu}^2}, \quad \not{M}_T \equiv \sqrt{\not{p}_T^2 + M_T^2}. \quad (3.2)$$

The conditional expectation values of M_{WW} for the given observables for the SM and at dimension-6 and dimension-8 are shown in figure 2. Of the four observables, the one which

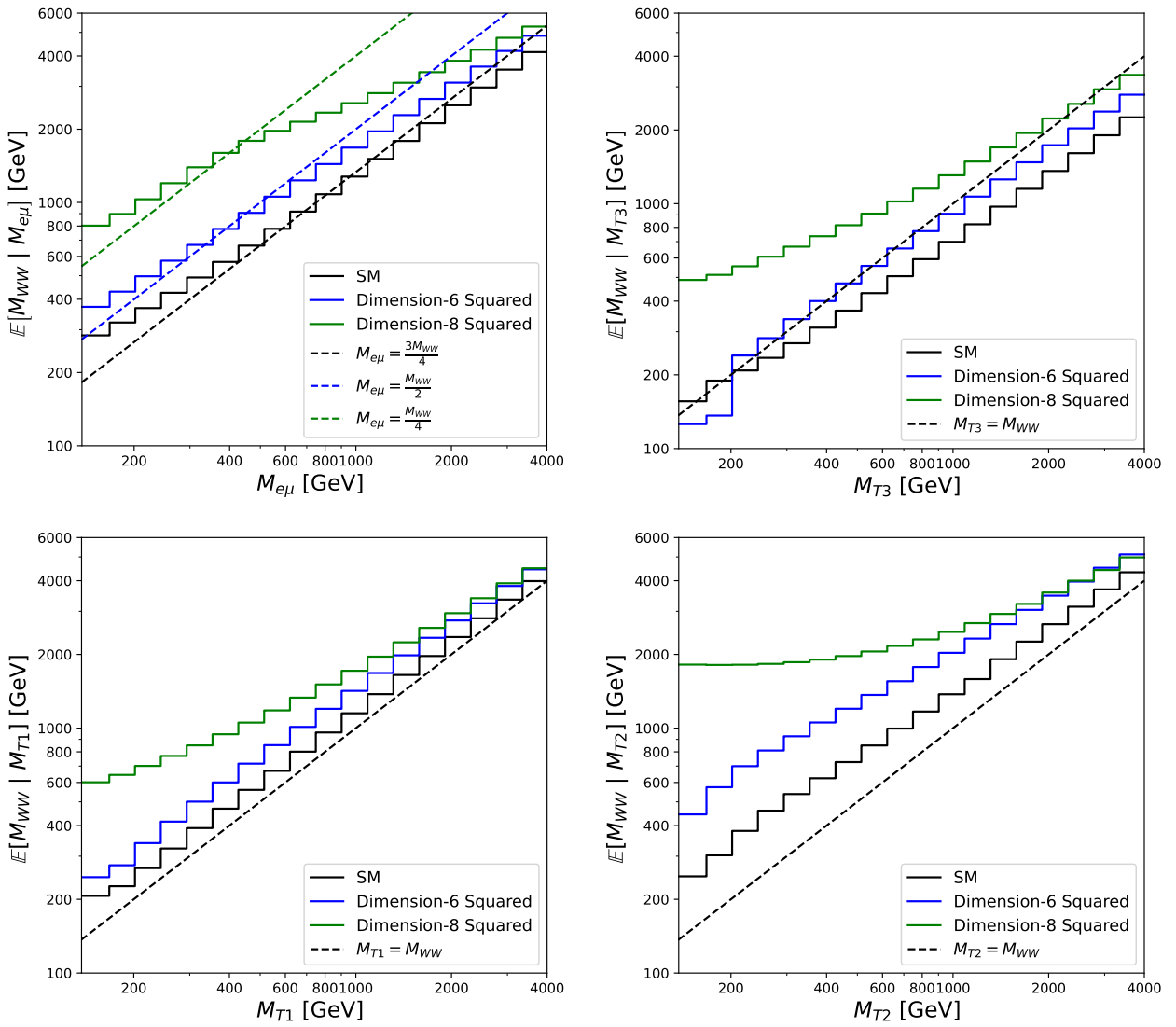


Figure 2: The conditional expectation value of M_{WW} for each bin of the $M_{e\mu}$ (top left), M_{T1} (bottom left), M_{T2} (bottom right), and M_{T3} (top right) distributions, for the SM (black), dimension-6 squared (blue), and dimension-8 squared (green) contributions. The error is given by calculating the asymmetric variance from the expectation value.

correlates best with M_{WW} is M_{T3} . We can also appreciate this fact by considering how the ratio between dimension-6 and dimension-8 compares with M^4/Λ^4 ($M = M_{T1}, M_{T2}, M_{T3}, M_{WW}$),

which should be of the order of magnitude of the ratio between dimension-6 and dimension-8, particularly for $M = M_{WW}$. We know this because the dimension-6 and dimension-8 squared contributions grow as M_{WW}^4/Λ^4 and M_{WW}^8/Λ^8 respectively. This is shown in figure 3. It can be seen that M_{T3} behaves the most closely to M_{WW} . In particular, it can be seen from figure 3, that $M_{e\mu}$ performs markedly worse as a proxy for M_{WW} .

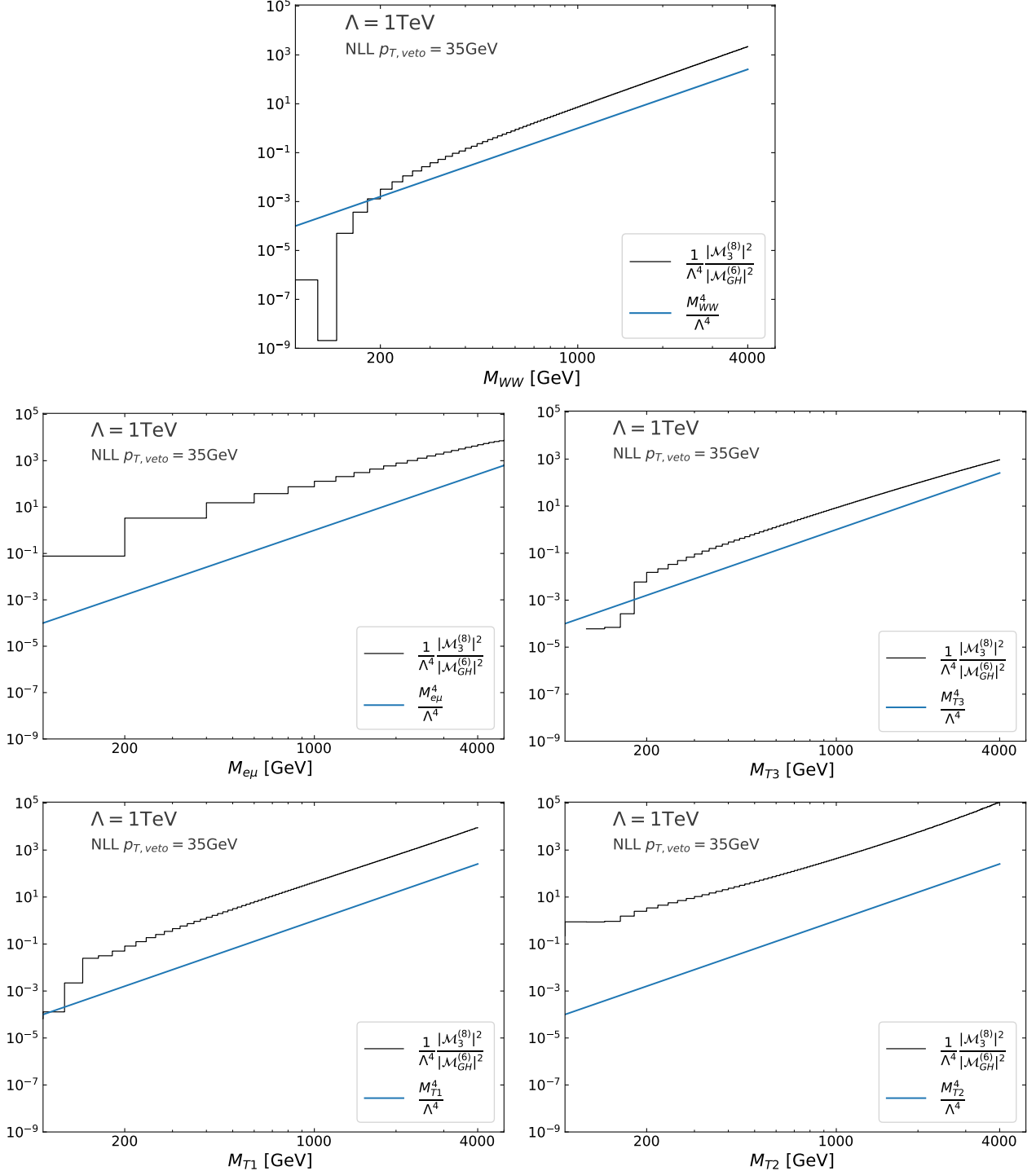


Figure 3: Comparison of the ratio of dimension-8 squared and dimension-6 squared contributions to the theoretical value from the EFT (for the M_{WW} distribution). This theoretical value is given as $\frac{M^4}{\Lambda^4}$, $M = \{M_{WW}, M_{T1}, M_{T2}, M_{T3}, M_{e\mu}\}$.

To have an indication of the values of $M_{e\mu}$ and M_{T3} for which the EFT breaks down at $\Lambda = 3$ TeV, in figure 4 we compare the relative sizes of dimension-6 quadratic, dimension-8 linear, and dimension-8 quadratic contributions for the $M_{e\mu}$ and M_{T3} distributions. We can see that the dimension-8 interference is still negligible in the region of validity of the EFT expansion for both M_{T3} and for $M_{e\mu}$. It can also be seen that the M_{T3} observable gives a larger range of bins where the EFT is valid for a given Λ . Also, since M_{T3} correlates so much better with M_{WW} , the Higgs peak appears at around the value of $M_{T3} = 125$ GeV, whereas for $M_{e\mu}$ it appears at energies $M_{e\mu} < 100$ GeV. In the following, we will focus only on the tails of the distributions, excluding any effect from the Higgs peak, and we only look at bins for $M_{T3} > 200$ GeV and $M_{e\mu} > 138$ GeV.

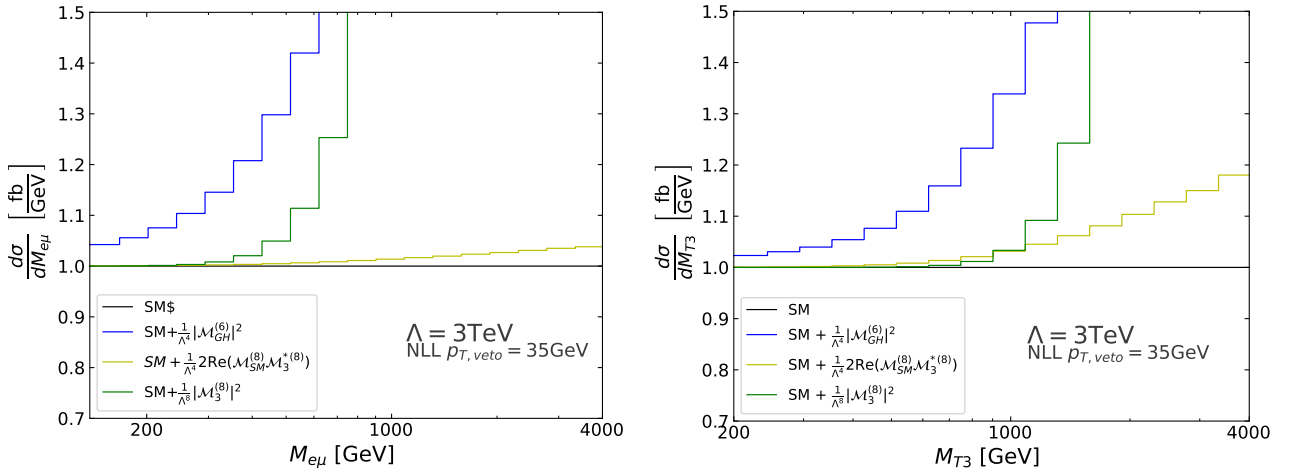


Figure 4: Comparison of M_{T3} and $M_{e\mu}$ distributions of SM (black) with SM theoretical uncertainty (shaded area), dimension-6 squared contribution (blue) and dimension-8 squared (green) and SM interference (yellow) contributions, for $\Lambda = 3$ TeV.

4 Sensitivity Studies

We can set constraints on new physics by using the cut on data (CoD) method outlined in the previous using M_{T3} as a proxy for M_{WW} . This ensures EFT validity for these constraints without needing to profile the size of dimension-8 operators. The cut can either be applied directly onto the M_{T3} distribution, or can be used with another distribution (e.g. in $M_{e\mu}$), by ensuring that the M_{T3} cut is added to the fiducial cuts of table 1. To compare the CoD method with the $M_{e\mu}$ distribution to what is in use by ATLAS (CoS), in figure 5 we plot the $M_{e\mu}$ distribution with the cut on data of $M_{T3} < 750$ GeV and the cut on simulation of dimension-6 at $M_{WW} < 750$ GeV for an EFT scale $\Lambda = 1$ TeV. In fact, using the M_{WW} distribution, we found that a more appropriate value for the CoD or CoS would have been at most 650 GeV. However, applying the cut $M_{T3} < 750$ GeV still keeps dimension-8 at or around the same level as dimension-6 for the CoD approach.

We then performed sensitivity studies to compare the method of CoS on the dimension-6 EFT simulation (at $M_{WW} < 750$ GeV), to the method of implementing a CoD at $M_{T3} < 750$ GeV. We compared both of these to the method of ensuring that dimension-6 is larger than dimension-8 bin by bin (CBB). We also investigated if we could obtain better constraints using the M_{T3} distribution when compared to constraints with the $M_{e\mu}$ distribution, both with the CBB method. We used pure NNLL predictions for the SM $q\bar{q}$ channel as this allowed us to use MCFM-RE, which was faster than computing the full NNLO+NNLL prediction with

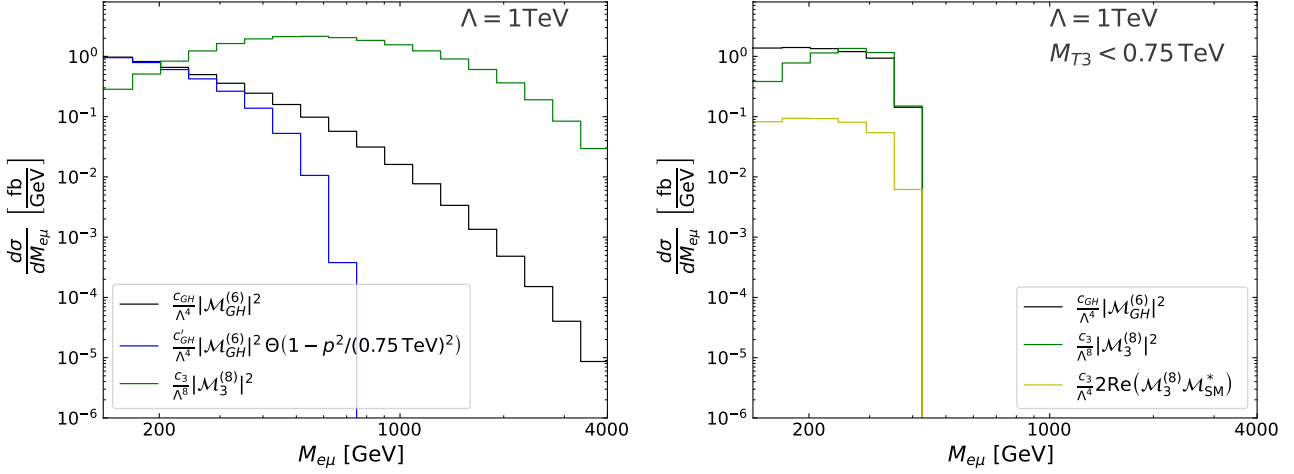


Figure 5: Comparison of the cut on simulation (CoS) approach (left) with the cut on data (CoD) approach (right). The CoD approach includes an extra fiducial cut of $M_{T3} < 0.75$ TeV whereas the CoS approach applies a cut of $M_{WW} < 0.75$ TeV only to the generation of dimension-6 EFT contributions. The dimension-6 contribution without CoS is shown in black. The dimension-6 contribution with CoS is shown in blue. Dimension-8 squared (green) and interference (yellow) contributions are also shown without a CoS.

MATRIX+RadISH. In [24], we showed that the agreement between the two predictions is within 5%, and with even better agreement at high values of $M_{e\mu}$ and M_{WW} . Since the SM gg contribution is heavily suppressed (< 5% of the $q\bar{q}$ contribution [24]) at high energies, we neglect it for this study. This is true for both the $M_{e\mu}$ and M_{WW} distributions, the latter of which should be correlated to the transverse mass observable M_{T3} . We do not take into consideration EW corrections which make these contour plots more conservative (as EW corrections give a large Sudakov suppression in the tails of the SM distribution).

For our sensitivity studies, we use the method of [24]. Using eq. (2.2) and our BSM prediction at NLL we can define, for a set of c_i and Λ , a prediction at the HL-LHC which we call $\{m_j(c_i, \Lambda)\}$. We can then compare this to data points $\{n_j\}$ obtained by drawing a Poisson distribution from the NNLL SM predictions. To ensure EFT validity, we only take $\{n_j\}$ bins, up to the largest bin N which satisfies eq. (1.2) for the given value of Λ .

For the generation of exclusion plots and sensitivity studies we then use a delta chi-squared test statistic defined as:

$$\Delta\chi^2(c_i, \Lambda) \equiv \chi^2(c_i, \Lambda) - \chi^2(\hat{c}_i, \hat{\Lambda}), \quad (4.1)$$

where $\chi^2(c_i, \Lambda)$ is defined as:

$$\chi^2(c_i, \Lambda) \equiv \sum_{j=1}^N \frac{(n_j - m_j(c_i, \Lambda))^2}{(\Delta m_j(c_i, \Lambda))^2}, \quad (4.2)$$

and \hat{c}_i and $\hat{\Lambda}$ are values which minimise $\chi^2(c_i, \Lambda)$. For each value of N , the \hat{c}_i and $\hat{\Lambda}$ must be found separately. In order to account for theoretical and systematic errors, following [25], we use

$$(\Delta m_j(c_i, \Lambda))^2 = m_j(c_i, \Lambda) + (\Delta_j^{(th)}/2)^2 + (\Delta_j^{(sys)}/2)^2. \quad (4.3)$$

In the above equation, $\Delta_j^{(th)}$ is the theoretical scale variation uncertainty associated with the BSM prediction m_j . The quantity $\Delta_j^{(sys)}$ gives an expected experimental systematic error at the HL-LHC, computed by extrapolating current systematic errors from ATLAS [14] to higher energies.

To obtain constraints for the HL-LHC sensitivity studies we use the method of median significance. This is done by generating many sets of $\{n_j\}$ using the expected $\{\bar{n}_j\}$ given by the Standard Model best prediction and a Poisson distribution for each bin independently. For these simulated data sets we obtain the probability distribution for $\Delta\chi^2(\{c_i, \Lambda\})$, whose median makes it possible to calculate the p-value associated with each considered $\{c_i, \Lambda\}$. We then exclude all values of $\{c_i, \Lambda\}$ whose p-value is less than 0.05. We then present results obtained by using 18 logarithmically spaced bins in the $M_{e\mu}$ distribution and the 16 logarithmically spaced bins in the M_{T3} distribution.

We note that when performing EFT constraints, we can only fit the combined factor c_i/Λ^n (with n determined by the dimension of the operator). There are two options for extracting constraints which is either to set $c_i = 1$ or fix Λ and extract constraints on c_i . The ideal scenario is to fit both simultaneously, with Λ determining the number of bins used in each fit for c_i giving full multidimensional constraints. However, for the purposes of comparison of methods, we fix $\Lambda = 1 \text{ TeV}$ and extract constraints on c_i .

First, we study clipping only the EFT simulation (CoS) (with no high energy cut on the data). We use the cuts $M_{WW} < \Lambda$ and $M_{WW} < 0.75\Lambda$ (equivalent to replacing c_i with $c_i\Theta(1 - p^2/(f\Lambda^2))$ with $f = \{0.75, 1\}$ respectively). We compare this procedure to using a cut of $M_{T3} < \Lambda$ and $M_{T3} < 0.75\Lambda$ directly on the data (CoD), and fitting the $M_{e\mu}$ distribution with those cuts. The corresponding contour plots are shown in figure 6. Although the CoD method is more conservative, it gives comparable bounds with respect to CoS. This is partly due to the fact that CoD acts on the SM background as well, thus increasing the relative size of BSM contributions. Also, the Wilson coefficients extracted with CoD have a clear interpretation in terms of a local EFT, which is not the case for CoS.

We can also compare CoS and CoD to the CBB method, i.e. setting $\Lambda = 1 \text{ TeV}$, and using eq. (1.2) to determine the EFT valid bins. The contours obtained with CBB applied to the $M_{e\mu}$ distribution are shown in the left panel of figure 7. It can be noted that CBB gives a more stringent condition on data than CoS and CoD with the current setup, leading to looser constraints on the Wilson coefficients. More stringent cuts on M_{WW} (for CoS) and M_{T3} (for CoD), e.g. $M_{WW}/M_{T3} < 650 \text{ GeV}$ lead to similar constraints.

The CBB method automatically ensures the validity of the EFT expansion. Once this is established, one can use the observable that provides the best sensitivity. In this case, this is $M_{e\mu}$, and not M_{T3} , despite the latter being better correlated to M_{WW} (see the right panel of figure 7). This is because the bins which are added in the EFT valid region for M_{T3} are at lower energies, where the sensitivity to higher dimensional operators is less pronounced (see figure 4). It is because M_{T3} is better correlated with M_{WW} that these lower energy regions receive much less BSM contributions than for $M_{e\mu}$. It should also be noted that the M_{T3} distribution uses two fewer bins than the $M_{e\mu}$ distribution.

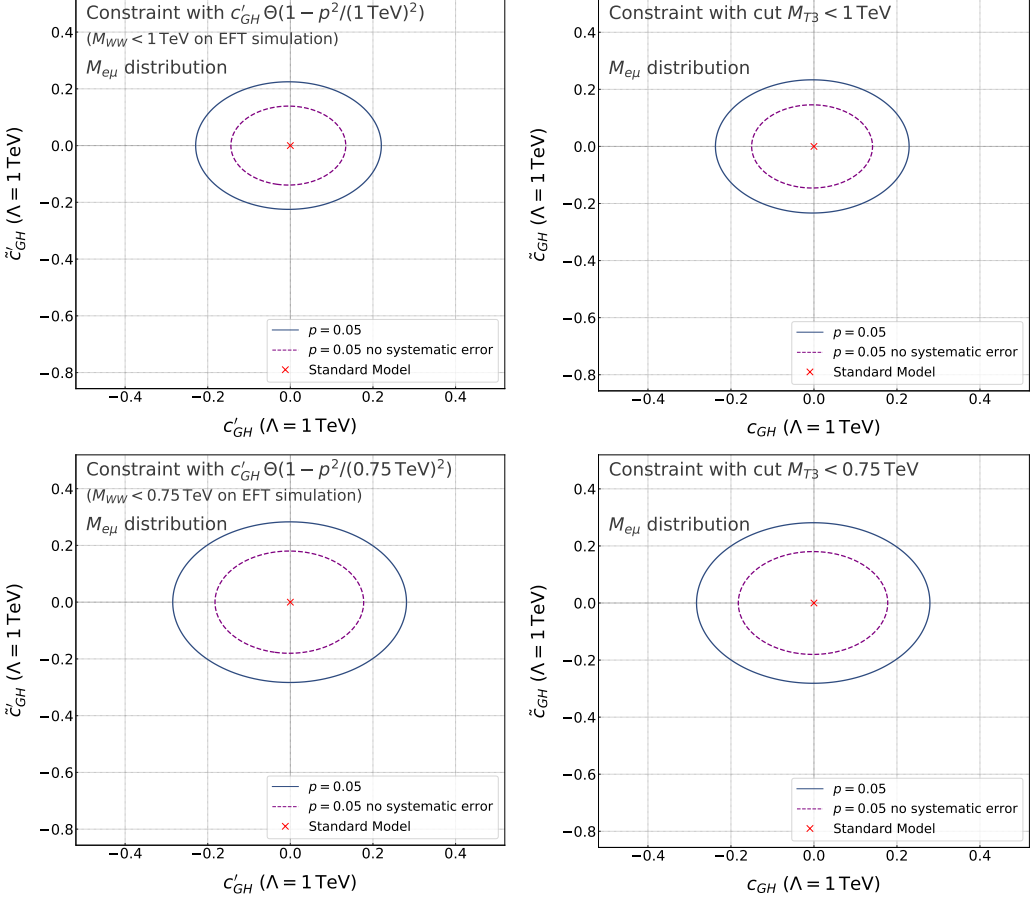


Figure 6: Sensitivity studies on the CP-even and CP-odd version of the dimension-6 operator ($\phi\phi GG$) performed on projected HL-LHC data. On the right, an experimental cut has been placed at $M_{T3} < \{1, 0.75\}$ TeV. On the left, the simulation has been clipped for the dimension-6 only such that $M_{WW} < \{1, 0.75\}$ TeV which is equivalent to modifying the SMEFT coefficient by a Heaviside function with transition at the relevant scale. The constraints are approximately the same between the two methods with a slightly stronger constraint for $M_{WW} < 0.75$ TeV than for the cut $M_{T3} < 0.75$ TeV.

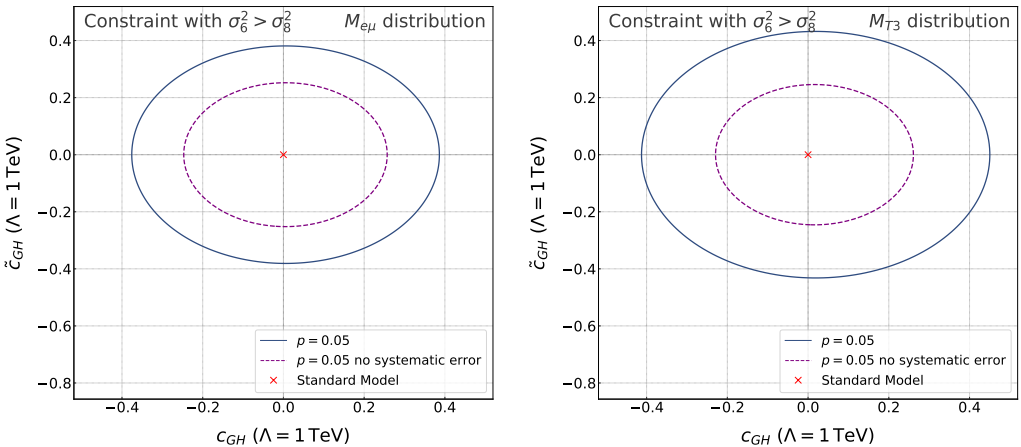


Figure 7: Sensitivity studies on the CP-even and CP-odd version of the dimension-6 operator ($\phi\phi GG$) performed on projected HL-LHC data. EFT validity is ensured by only using bins for which dimension-6 squared contribution is larger than the dimension-8 squared contribution. On the left the $M_{e\mu}$ distribution is used to make fits whereas on the right the M_{T3} distribution is used.

5 Conclusions

In this letter, we have addressed the question of how to probe higher dimensional operators in WW production, while still ensuring that the EFT expansion is valid. This is more challenging than in other channels, because we do not have direct access to the invariant mass of the WW pair M_{WW} , which determines the relative size of different orders in the EFT expansion. In particular, we have considered fully leptonic WW production via gluon fusion, and the distribution in the dilepton invariant mass $M_{e\mu}$, which is used in all experimental analyses. As a case study, we probed the relative contributions of a dimension-6 operator which added a ggh contact interaction and a dimension-8 operator which adds a $ggWW$ contact interaction, already studied in [24]. Both operators give amplitudes which grow with energy, and can be constrained by studying the tails of the $M_{e\mu}$ distribution. Note that a similar analysis can be applied to higher-dimensional operators in the $q\bar{q}$ channel, which will be subject of future work.

First, we have observed that, naively imposing a cut on M_{WW} at the generator level to obtain information on the bins in $M_{e\mu}$ that can be safely used to obtain constraints on dimension-6 operators, does not eliminate the contribution of dimension-8 operators. In particular, there are bins in $M_{e\mu}$ where the latter dominate, thus invalidating the EFT expansion. Its validity can be restored only by manually selecting the bins where dimension-6 operators give the largest contribution. This unfortunately, restricts the constraining power of such analyses.

This is ultimately due to the poor correlation between $M_{e\mu}$ and M_{WW} . We have then considered three alternative variables, M_{T1} , M_{T2} and M_{T3} , and shown that M_{T3} has the best correlation with M_{WW} . Imposing a cut on M_{T3} identifies the region in which the EFT is valid in a way that can be implemented at the experimental level, i.e. directly on the data. This in turn makes it possible to investigate observables that have better sensitivity to higher operators, while remaining the region of EFT validity.

We finally remark that adding $M_{WW} < \Lambda$ cuts only to the EFT simulation could be interpreted as modifying the SMEFT expansion by a form factor and could impact the model independence of EFT fits under this procedure. Instead, imposing a cut on M_{T3} identifies the region in which the EFT is valid in a way that can be implemented at the experimental level, i.e. directly on the data. This in turn makes it possible to investigate observables that have better sensitivity to higher operators, while remaining the region of EFT validity.

Acknowledgements

We thank Ennio Salvioni, Jonas Lindert, Tom Gent, Charlie Hogg, Xavier Pritchard, Marco Sebastianutti, Lewis Mazzei, and Claudia Muni for useful discussions. AB is supported by the UK STFC under the Consolidated Grant ST/X000796/1, and thanks Royal Holloway, University of London for hospitality while this work was completed. The work of AM is partially supported by the National Science Foundation under Grant Number PHY-2412701. We acknowledge the use of computing resources made available by the Cambridge Service for Data Driven Discovery (CSD3), part of which is operated by the University of Cambridge Research Computing on behalf of the STFC DiRAC HPC Facility (www.dirac.ac.uk). The DiRAC component of CSD3 was funded by BEIS capital funding via STFC capital grants ST/P002307/1 and ST/R002452/1 and STFC operations grant ST/R00689X/1. DiRAC is part of the UK National e-Infrastructure.

References

- [1] Ilaria Brivio and Michael Trott. The Standard Model as an Effective Field Theory. *Phys. Rept.*, 793:1–98, 2019.
- [2] B. Grzadkowski, M. Iskrzynski, M. Misiak, and J. Rosiek. Dimension-Six Terms in the Standard Model Lagrangian. *JHEP*, 10:085, 2010.
- [3] Ilaria Brivio et al. Truncation, validity, uncertainties. 1 2022.
- [4] Hesham El Faham, Giovanni Pelliccioli, and Eleni Vryonidou. Triple-gauge couplings in LHC diboson production: a SMEFT view from every angle. *JHEP*, 08:087, 2024.
- [5] A. Azatov, D. Barducci, and E. Venturini. Precision diboson measurements at hadron colliders. *JHEP*, 04:075, 2019.
- [6] Ilaria Brivio, Yun Jiang, and Michael Trott. The SMEFTsim package, theory and tools. *JHEP*, 12:070, 2017.
- [7] Aleksandr Azatov, Roberto Contino, Camila S. Machado, and Francesco Riva. Helicity selection rules and noninterference for BSM amplitudes. *Phys. Rev. D*, 95(6):065014, 2017.
- [8] Céline Degrande and Hao-Lin Li. Impact of dimension-8 SMEFT operators on diboson productions. *JHEP*, 06:149, 2023.
- [9] Hesham El Faham, Giuseppe Ventura, and Eleni Vryonidou. Diboson production in the SMEFT at dimension-8. 11 2025.
- [10] Adam Martin. A case study of SMEFT $\mathcal{O}(1/\Lambda^4)$ effects in diboson processes: $pp \rightarrow W^\pm(\ell^\pm\nu)\gamma$. *JHEP*, 05:223, 2024.
- [11] Georges Aad et al. Measurements of W^+W^- production cross-sections in pp collisions at $\sqrt{s} = 13$ TeV with the ATLAS detector. 5 2025.
- [12] Measurement of the photon-fusion production cross section of a pair of W bosons. 7 2025.
- [13] Albert M Sirunyan et al. W^+W^- boson pair production in proton-proton collisions at $\sqrt{s} = 13$ TeV. *Phys. Rev. D*, 102(9):092001, 2020.
- [14] Morad Aaboud et al. Measurement of fiducial and differential W^+W^- production cross-sections at $\sqrt{s} = 13$ TeV with the ATLAS detector. *Eur. Phys. J. C*, 79(10):884, 2019.
- [15] Albert M. Sirunyan et al. Measurements of properties of the Higgs boson decaying to a W boson pair in pp collisions at $\sqrt{s} = 13$ TeV. *Phys. Lett. B*, 791:96, 2019.
- [16] Morad Aaboud et al. Search for heavy resonances decaying into WW in the $e\nu\mu\nu$ final state in pp collisions at $\sqrt{s} = 13$ TeV with the ATLAS detector. *Eur. Phys. J. C*, 78(1):24, 2018.
- [17] Morad Aaboud et al. Measurement of the W^+W^- production cross section in pp collisions at a centre-of-mass energy of $\sqrt{s} = 13$ TeV with the ATLAS experiment. *Phys. Lett. B*, 773:354–374, 2017.
- [18] Morad Aaboud et al. Search for diboson resonances with boson-tagged jets in pp collisions at $\sqrt{s} = 13$ TeV with the ATLAS detector. *Phys. Lett. B*, 777:91–113, 2018.

- [19] Morad Aaboud et al. Search for WW/WZ resonance production in $\ell\nu qq$ final states in pp collisions at $\sqrt{s} = 13$ TeV with the ATLAS detector. *JHEP*, 03:042, 2018.
- [20] Riccardo Bellan et al. A sensitivity study of VBS and diboson WW to dimension-6 EFT operators at the LHC. *JHEP*, 05:039, 2022.
- [21] Shankha Banerjee, Daniel Reichelt, and Michael Spannowsky. Electroweak corrections and EFT operators in $W+W-$ production at the LHC. *Phys. Rev. D*, 110(11):115012, 2024.
- [22] Johannes Bellm, Stefan Gieseke, Nicolas Greiner, Gudrun Heinrich, Simon Plätzer, Christian Reuschle, and Johann Felix von Soden-Fraunhofen. Anomalous coupling, top-mass and parton-shower effects in W^+W^- production. *JHEP*, 05:106, 2016.
- [23] Adam Falkowski, Martin Gonzalez-Alonso, Admir Greljo, David Marzocca, and Minho Son. Anomalous Triple Gauge Couplings in the Effective Field Theory Approach at the LHC. *JHEP*, 02:115, 2017.
- [24] Daniel Gillies, Andrea Banfi, Adam Martin, and Matthew A. Lim. Dimension-8 operators in $W+W-$ production via gluon fusion. *JHEP*, 06:111, 2025.
- [25] Luke Arpino, Andrea Banfi, Sebastian Jäger, and Nikolas Kauer. BSM WW production with a jet veto. *JHEP*, 08:076, 2019.
- [26] John M. Campbell and R. Keith Ellis. An Update on vector boson pair production at hadron colliders. *Phys. Rev. D*, 60:113006, 1999.
- [27] John M. Campbell, R. Keith Ellis, and Ciaran Williams. Vector Boson Pair Production at the LHC. *JHEP*, 07:018, 2011.
- [28] John M. Campbell, R. Keith Ellis, and Walter T. Giele. A Multi-Threaded Version of MCFM. *Eur. Phys. J. C*, 75(6):246, 2015.
- [29] Valerio Bertone, Stefano Carrazza, Nathan P. Hartland, and Juan Rojo. Illuminating the photon content of the proton within a global PDF analysis. *SciPost Phys.*, 5(1):008, 2018.
- [30] Richard D. Ball et al. The path to proton structure at 1% accuracy. *Eur. Phys. J. C*, 82(5):428, 2022.